Supporting Information

Chang et al. 10.1073/pnas.1103411108

SI Results

Definitions of Terms Used in Replication Compartments Tracking and Trajectory Analysis. ***Trajectory.*** A track connecting the 3D positions of an object [in this example, individual replication compartments (RCs)] at each time point within a time series. A trajectory represents the path of the movement of an object.

Mean square displacement. Mean square displacement (MSD) is a measure of the average distance of the movement of an object. The shape of the MSD curve over time indicates the motion type.

Simple diffusion. Simple diffusion is the typical diffusion process where the MSD increases linearly with time.

Directed motion. Directed motion is a superdiffusive process where the MSD increases faster than linearly with time.

Anomalous diffusion. Anomalous diffusion is a subdiffusive process where the MSD increases slower than linearly with time.

Anomalous diffusion coefficient (α). The anomalous diffusion coefficient is the parameter that describes the deviation from linearity of the MSD curve over time.

Obstructed and confined diffusion. Obstructed and confined diffusion are subclasses of anomalous diffusion (subdiffusive process) where the MSD increases slower than linearly with time. Obstructed and confined diffusion can be further classified based on the anomalous diffusion coefficient: $0.1 \leq \alpha < 0.9$ for obstructed diffusion and $\alpha < 0.1$ for confined diffusion.

3D relative shape anisotropy (κ^2). This parameter is used to characterize the 3D shape of a trajectory. Directed motion corresponds to trajectories with a more elongated or anisotropic shape (κ^2 values are close to one). Simple diffusion (or random motion) corresponds to trajectories with a more spherical or isotropic shape (κ^2 values close to zero).

Ellipsoid of gyration. An ellipsoid of gyration is an ellipsoid that characterizes the asymmetry of a trajectory. The semiaxes of the ellipsoid correspond to the principal axes of the trajectory (collection of 3D positions). The elongation or anisotropy of the ellipsoid is determined by the lengths of its semiaxes.

SI Experimental Procedures

Plasmids Used for Transfections. Plasmids encoding nuclear myosin I (NMI) -E407V, actin-G13R, and actin-NLS are described in refs. 1 and 2. The mCherry-lamin A plasmid (mCh-LA) used for tracking nuclear position is described in ref. 3. The mCh-SC35 plasmid was constructed by excising the SC35 ORF of a pCMV-YPF-N1-SC35 plasmid (4) and subcloning it into an mCherry-N1 vector.

4D Tracking. We developed fully automated approaches for image registration as well as tracking of multiple replication compartments. Briefly, to remove the translational and rotational motion of the nucleus (visualized by the mCh-LA localization), we developed a rigid registration approach. With this approach, the following steps were carried out. For each time step of an image sequence, we detected the image region corresponding to the nucleus using a 3D Gaussian filter and an intensity threshold. The values for the SDs σ_{xy} and σ_z of the Gaussian filter were chosen based on the size of the nucleus (typically, we used values of $\sigma_{xy} = 10$ and $\sigma_z = 2$ voxels). The position of the nucleus was determined by computing the center of mass of the corresponding voxel positions, whereas the orientation was obtained by diagonalizing the covariance matrix of the voxel positions. Each time step t of the image sequence was aligned to time step zero by computing a rigid transformation based on the position and orientation of the nucleus at both time steps. Subsequently, we applied an intensity-based rigid registration scheme (5). Because of photobleaching, the intensities of the first time step differed strongly from those of the latter time steps. Without proper compensation for this variation, finding a correct transformation between the first and latter time steps based on their intensities may be challenging. To cope with this, we applied the registration approach to consecutive time steps of the image sequence, thereby obtaining a rigid transformation between time steps t and $t + 1$. By recursively concatenating the sequential transformations, we computed the required transformation between time steps zero and t. We applied this registration approach to the images in the mCherry channel. The resulting transformations were also applied to the corresponding images in the GFP channel. We used the registered 3D image sequences as input for the tracking approach. For tracking multiple replication compartments, we developed a probabilistic approach (6). At each time step of an image sequence, our approach performs four steps: (*i*) detection and localization of compartments, (*ii*) prediction of the position of the tracked compartments, (*iii*) matching of the predicted positions with the detected compartments, and (*iv*) estimation of position. To detect and localize the compartments, image regions corresponding to the objects of interest were enhanced using a 3D Laplacian of Gaussian filter (7, 8). The values for the SDs σ_{xy} and σ_z of the filter were chosen based on the size of the compartments (usually, we used values of $\sigma_{xy} = 5$ and $\sigma_z = 3$ voxels). After filtering, an intensity threshold was computed from the mean intensity of the image plus a factor $c \times$ SD of the image intensities; the threshold was applied to the image to detect regions corresponding to compartments. To identify these regions, we used a connected components-labeling algorithm (six connectivity), which groups spatially adjacent detected voxels by analyzing the local neighborhood (consisting of six voxels) around each considered voxel. The position of each compartment was determined by computing the center of mass. To calculate a prediction for the position of each tracked compartment, we used a spatial–temporal filter (in this case, a Kalman filter with a Brownian motion model). To find the correspondence between a predicted position and a detected compartment, we used a global nearest-neighbor approach (9). Based on the predicted and detected position estimates, the final position estimate of a tracked compartment was computed using the spatial–temporal filter.

RC Motion Analysis. To determine the motion type of individual compartments, we developed a hierarchical approach based on both the anomalous diffusion coefficient α (10) as well as the 3D relative anisotropy κ^2 (11, 12). To obtain an estimate for the anomalous diffusion coefficient (α) of a trajectory, we computed the MSD as a function of the time interval Δt. We fitted the anomalous diffusion model $\mathrm{MSD} = 6D\Delta t^{\alpha}$ (10) to the calculated MSD values, thereby obtaining an estimate for the diffusion coefficient D as well as the anomalous diffusion coefficient α. To improve the accuracy of the estimates (10), we restricted the MSD calculations to time intervals Δt smaller than $N/3$, where N is the total number of available positions in the trajectory. To characterize the shape of the trajectory by its 3D relative anisotropy κ^2, we first calculated the squared radius of gyration s^2, the asphericity b, and the acylindricity c using the eigenvalues of the covariance matrix of the trajectory's positions. Based on these shape measures, we calculated the relative shape anisotropy $\kappa^2 = (b^2 + 0.75c^2)/s^4$. Note that $\kappa^2 \in [0, 1]$, where values close to 0 correspond to trajectories with an isotropic shape (i.e., trajectories exhibiting random motion), whereas values

tending to one correspond to trajectories with an anisotropic shape (i.e., trajectories displaying directed motion). Thus, we used κ^2 as our criterion to detect directed motion using a threshold value of $\kappa^2 = 0.5$. This threshold value was determined using simulated trajectories where the true motion type of the trajectories was known. Our hierarchical approach for determining the motion type of the compartments, therefore, first used κ^2 to distinguish trajectories exhibiting directed motion from those displaying random motion. We then used the scheme proposed by Bacher et al. (13) to classify the latter into confined diffusion ($\alpha < 0.1$), obstructed diffusion ($0.1 \leq \alpha < 0.9$), or simple diffusion ($\alpha \geq 0.9$). An average of four nuclei per treatment were analyzed for MSD and anisotropy analyses (~22 RCs per treatment). A two-sample Kolmogorov–Smirnov test (14) was used to determine the statistical significance of differences between experimental groups in cumulative distribution of κ^2 values.

Antibodies Used for Indirect Immunofluorescence and Western Blot Experiments. For the indirect immunofluorescence studies, mouse anti-SC35 (clone SC-35, S4045, 1:1,000 dilution; Sigma-Aldrich) and rabbit anti-ICP8 (3-83, 1:500 dilution) (15) antibodies were used. Goat anti-mouse Alexa 594 (Invitrogen) and goat anti-rabbit Alexa 488 (Invitrogen) were used at a 1:500 dilution for secondary detection.

Antibodies used in Western blot experiments were mouse anti-ICP27 (H1A027, 1:2,500 dilution; EastCoast Bio), rabbit anti-ICP8 (3-83, 1:10,000 dilution) (15), mouse anti-gC (H1A022, 1:2,500 dilution; Virusys), and mouse anti-GAPDH (G041, 1:5,000 dilution, Applied Biological Materials). HRP-conjugated goat antibodies were used at 1:10,000 dilution (Santa Cruz Biotechnology).

Sequences of Primers Used in RNA to CT One-Step Quantitative PCR and Standard Quantitative PCR Reactions.

ICP27 (mRNA): 5′-GATTCGGGCCCGGTCGTTGCTAC-3′, 5′-CCGTCGGGGCTGGGGTGTC-3′.
ICP27 (gene): 5′-CCGCCGGCCTGGATGTGACG-3′, 5′-CGTGGTGGCCGGGGTGGTGCTC-3′ (16).
ICP8 (mRNA): 5′-CCCAGCACCCAGGCCCCAAACC-3′, 5′-AGCGCCTCCCCCGTCGTCTCGT-3′.
gC (mRNA): 5′-CCCCCGCGGACCTTCACCT-3′, 5′-GGCCGCGGCAGCACCAG-3′.
ICP5 (mRNA): 5′-CTTAGCACGATCGAGGT-3′, 5′-GTTCATGTAGGCCAGCT-3′.
18s rRNA (RNA): 5′-CATGAACGAGGAATTCCCAGTAA-3′, 5′-GATCCGAGGGCCTCACTAAAC-3′ (17).
Sonic hedgehog (gene): 5′-CTGATCGATCGTGGGGGTTATGTG-3′, 5′-TGCGGGCGTCAGGGTGGAT-3′.

1. Chuang CH, et al. (2006) Long-range directional movement of an interphase chromosome site. *Curr Biol* 16:825–831.
2. Posern G, Sotiropoulos A, Treisman R (2002) Mutant actins demonstrate a role for unpolymerized actin in control of transcription by serum response factor. *Mol Biol Cell* 13:4167–4178.
3. Taimen P, et al. (2009) A progeria mutation reveals functions for lamin A in nuclear assembly, architecture, and chromosome organization. *Proc Natl Acad Sci USA* 106: 20788–20793.
4. Prasanth KV, Sacco-Bubulya PA, Prasanth SG, Spector DL (2003) Sequential entry of components of the gene expression machinery into daughter nuclei. *Mol Biol Cell* 14: 1043–1057.
5. Yang S, et al. (2008) Nonrigid registration of 3-d multichannel microscopy images of cell nuclei. *IEEE Trans Image Process* 17:493–499.
6. Godinez WJ, et al. (2009) Deterministic and probabilistic approaches for tracking virus particles in time-lapse fluorescence microscopy image sequences. *Med Image Anal* 13: 325–342.
7. Marr D, Hildreth E (1980) Theory of edge detection. *Proc R Soc Lond B Biol Sci* 207: 187–217.
8. Sage D, Neumann FR, Hediger F, Gasser SM, Unser M (2005) Automatic tracking of individual fluorescence particles: Application to the study of chromosome dynamics. *IEEE Trans Image Process* 14:1372–1383.
9. Sbalzarini IF, Koumoutsakos P (2005) Feature point tracking and trajectory analysis for video imaging in cell biology. *J Struct Biol* 151:182–195.
10. Saxton MJ, Jacobson K (1997) Single-particle tracking: Applications to membrane dynamics. *Annu Rev Biophys Biomol Struct* 26:373–399.
11. Theodorou DN, Suter UW (1985) Shape of unpreturbed linear polymers: Polypropylene. *Macromolecules* 18:1206–1214.
12. Saxton MJ (1993) Lateral diffusion in an archipelago. Single-particle diffusion. *Biophys J* 64:1766–1780.
13. Bacher CP, Reichenzeller M, Athale C, Herrmann H, Eils R (2004) 4-D single particle tracking of synthetic and proteinaceous microspheres reveals preferential movement of nuclear particles along chromatin—poor tracks. *BMC Cell Biol* 5:45.
14. Conover WJ (1971) One-sample "Komogorov" test/two-sample "Smirnov" test. *Practical Nonparametric Statistics*, ed Wiley B (Wiley, New York), pp 295–314.
15. Knipe DM, Senechek D, Rice SA, Smith JL (1987) Stages in the nuclear association of the herpes simplex virus transcriptional activator protein ICP4. *J Virol* 61:276–284.
16. Cliffe AR, Garber DA, Knipe DM (2009) Transcription of the herpes simplex virus latency-associated transcript promotes the formation of facultative heterochromatin on lytic promoters. *J Virol* 83:8182–8190.
17. Wright PJ, Crameri G, Eaton BT (2005) RNA synthesis during infection by Hendra virus: An examination by quantitative real-time PCR of RNA accumulation, the effect of ribavirin and the attenuation of transcription. *Arch Virol* 150:521–532.

Table S1. Statistical analysis of the distribution of κ^2 values in different experimental groups

Group I	Group II	*P* value*
Control	BDM	0.011
Control	Latrunculin A	0.006
Control	NMI-E407V	0.001
Control	Actin-G13R	0.013
Control	Actin-NLS	0.038
Actin-G13R	Actin-NLS	0.395
NMI-E407V	Actin-NLS	0.208
Control	α-amanitin	0.002
Control	Cycloheximide	0.355
α-amanitin	Cycloheximide	0.024
BDM	Latrunculin A	0.74
BDM	α-amanitin	0.221
Latrunculin A	α-amanitin	0.674
NMI-E407V	Actin-G13R	0.897
BDM	NMI-E47V	0.892
Latrunculin A	Actin-G13R	0.781

*P value based on the comparison of κ^2 values of Group I vs. Group II as determined by a Kolmogorov–Smirnov test. An average of 4 nuclei and 22 RCs were analyzed per treatment.

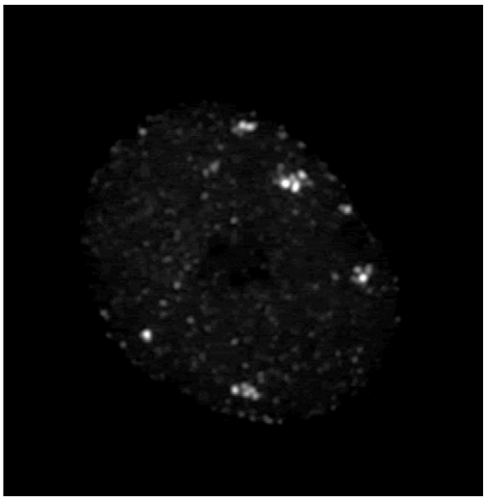

Movie S1. A maximum intensity projection movie of a cell that has been infected with the ICP8-GFP virus for 4 h is shown. A *z*-stack image was captured every 30 s for 3 h.

Movie S1

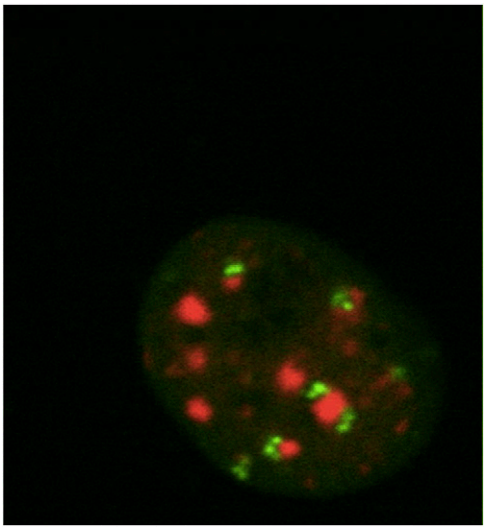

Movie S2. A cell transfected with mCherry-SC35 for 24 h and infected with the ICP8-GFP virus is shown. The movie was captured at 4 hpi every 30 s for 79.5 min. SC35 is shown in red, and ICP8 is in green.

Movie S2

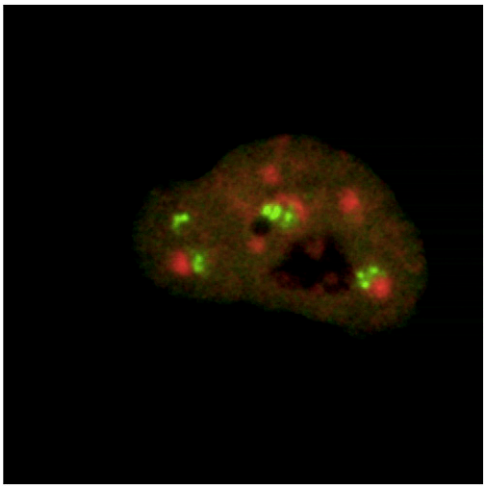

Movie S3. A cell transfected with mCherry-SC35 for 24 h and infected with the ICP8-GFP virus is shown. At 3 hpi, the cell was treated with latrunculin A (lat A) and imaged at 4 hpi with 30-s time intervals for 58 min. SC35 is shown in red, and ICP8 is in green.

Movie S3

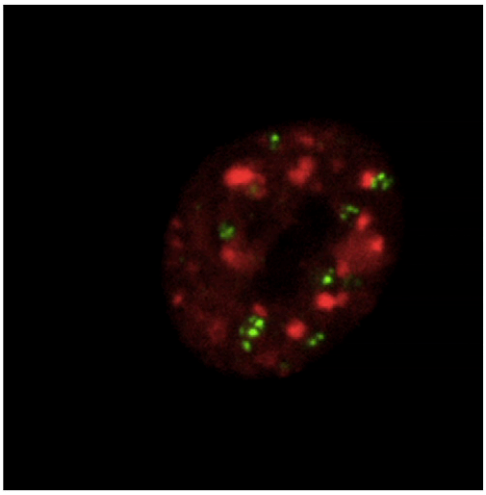

Movie S4. A cell transfected with mCherry-SC35 for 24 h and infected with the ICP8-GFP virus is shown. At 3 hpi, the cell was treated with 2,3-butanedione monoxime (BDM) and imaged at 4 hpi with 30-s time intervals for 90 min. SC35 is shown in red, and ICP8 is in green.

Movie S4

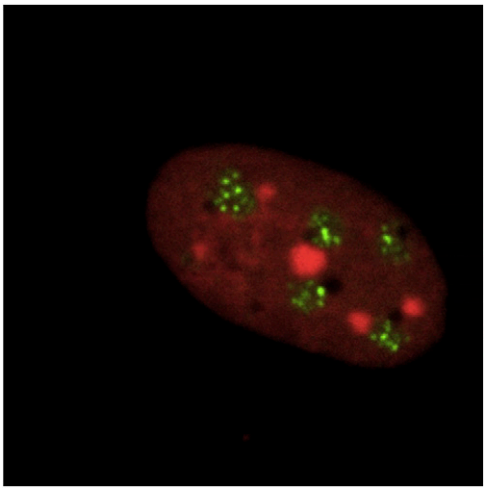

Movie S5. A cell transfected with mCherry-SC35 for 24 h and infected with the ICP8-GFP virus is shown. At 4 hpi, the cell was treated with α-amanitin and imaged immediately thereafter, with 30-s time intervals, for 90 min. SC35 is shown in red, and ICP8 is in green.

Movie S5